Disclination loops in Ni-Mo amorphous alloy films induced by ion irradiation

1991 J. Phys.: Condens. Matter 3 5769

(http://iopscience.iop.org/0953-8984/3/31/001)

J. Phys.: Condens. Matter 3 (1991) 5769–5781. Printed in the UK

Disclination loops in Ni–Mo amorphous alloy films induced by ion irradiation

B X Liu†, C H Shang and H D Li

Department of Materials Science and Engineering, Tsinghua University, Beijing 100084, People's Republic of China

Received 11 September 1990, in final form 19 March 1991

Abstract. Ni–Mo amorphous films were obtained by 200 keV xenon ion mixing at room temperature to dosages higher than 7×10^{14} ion cm^{-2}. It was found, for the first time, that when the irradiation dose went up to 7×10^{15} ion cm^{-2}, many odd lines appeared in the amorphous matrix. After excluding various possible explanations, we attribute the observed loops to line defects, i.e. disclinations in amorphous solids. Rich microstructures pertinent to disclination loops are described in detail. Scaling analysis showed that the observed disclinations shared a common fractal dimension in the small length scale. Moreover, approximation of gauge theory in the limit of elastic continuum media enables us to account for their anomalous properties successfully.

1. Introduction

Dislocations are a ubiquitous form of line defect in crystalline solids, controlling many of their mechanical properties [1]. The probable existence of similar defects in amorphous materials has been a long-standing argument which has aroused considerable interest among condensed matter physicists [2]. The topological study of amorphous structures in terms of SO(3) gauge theory [3] showed that dislocations of any kind are not structurally stable in amorphous elastic continua; instead it was proposed that an additional type of line defect, i.e. a rotational 2π disclination, exists as a single structurally stable constituent $Z_2\Pi_1(\mathrm{SO}(3))$ in amorphous solids. The existence of disclinations allows one to speculate whether the liquid, crystalline, quasi-crystalline and amorphous states differ largely in the spatial organization and kinetics of such line defects [4]. To our knowledge, however, no direct evidence for such line defects in metallic glasses has ever been reported up until now, which makes this prospective approach remain a pedagogical discussion. Therefore, direct observation of disclination loops in amorphous states is of great importance from both the theoretical and experimental points of view. In this paper, we present, for the first time, strong evidence for the existence of such line defects, and discuss theoretically some items concerning the observed disclination loops. We hope our observations will stimulate increasing interest in this issue.

---

† Also at Centre of Condensed Matter and Radiation Physics CCAST (World Lab.), Beijing, China.

0953-8984/91/315769+13$03.50

2. Experimental procedure

Ni–Mo multilayered films were prepared by alternatively depositing three layers of Ni and two layers of Mo metals onto SiO_2 wafers with a glass-like surface in a high vacuum system. The vacuum level during deposition was 5×10^{-7} Torr. The overall composition and thickness of the deposited films were confirmed to be $Ni_{65}Mo_{35}$ and 42 nm, respectively, by Rutherford backscattering (RBS) measurement. Ion mixing was conducted at room temperature by using 200 keV scanning xenon ions to obtain high efficiency. More than ten doses were designed to cover the range from $1\text{–}100 \times 10^{14}$ ion cm^{-2}. The beam current density was maintained at less than 1 μA cm^{-2} to minimize the beam heating. The vacuum level during irradiation was better than 1×10^{-6} Torr. The details of the experiment can be found in [5]. X-ray analysis was conducted in a D/max-IIIA diffractometer with an attachment for high sensitivity for thin film analysis. The samples were also checked by RBS measurements to unravel the configuration of the thin films, and to characterize the mixing efficiency induced by the ion irradiation. The resistive features of the solid films were measured by a standard four-point probe. For transmission electron microscopy (TEM, JEM-200CX and H-800, operated at 200 keV) examination, self-supported films were obtained by eroding the SiO_2 substrates in the HF acid, then cleaned in de-ionized water, and finally put onto the Cu grids. Selected area diffraction (SAD), *in situ* scanning electron microscopy (SEM), and energy dispersive spectroscopy (EDS) were also used to characterize the microstructure of the films.

3. Main results and contrast formulation

3.1. Formation of amorphous films

Figure 1 illustrates a set of backscattering spectra. As indicated in figure 1, the multilayered structures, i.e. three layers of Ni and two layers of Mo, were clearly shown in both the as-deposited samples and irradiated ones when the irradiation dose was lower than 7×10^{14} ion cm^{-2}. It can also be seen that the amplitude reflecting the structural oscillation decreased continuously with an increase in the ion fluence, and when the dosage reached 7×10^{14} ion cm^{-2}, all the zigzag vibration peaks were smeared out. These results clearly indicated that when the dosage was 7×10^{14} ion cm^{-2} and above, the Ni and Mo atoms were homogeneously mixed in the films. All the samples were also examined by x-ray diffraction to reveal the phase structures in the films. The diffraction results shown in figure 2 demonstrate that the dosage of 7×10^{14} ion cm^{-2} just corresponds to the dosage necessary to vitrify the films. When the irradiation dose was less than 7×10^{14} ion cm^{-2}, the two strongest diffraction peaks, i.e. Mo (110) and Ni (111), could be easily identified, indicating that the films were in a polycrystalline state. However, in other cases, as shown in figures 2(*d*)–(*e*), only widely spread halos could be recorded, which meant that the Ni–Mo alloys were uniformly vitrified as the irradiation dose equalled or exceeded 7×10^{14} ion cm^{-2}. The same amorphization procedure was also confirmed by the electron diffraction experiment by means of TEM. Four-point probe resistivity measurements again showed that the dose of 7×10^{14} ion cm^{-2} was the lowest one to saturate the sheet resistivity [6] at about 150 $\mu\Omega$ cm. Following the diffraction patterns shown in figures 2(*a*)–(*c*), it can be deduced that, with an increase in ion fluence, an increasing number of Ni atoms collided with the Mo lattice, and *vice versa*, which resulted in the two characteristic diffraction peaks moving toward each other and eventually overlapping. When a dose of 7×10^{14} ion cm^{-2} was reached, the two seriously distorted lattices, FCC and BCC, were intrinsically destabilized and transformed into a new atomic configuration, i.e. an amorphous structure. By now the essential point is that when the irradiation dosage was higher than or equal to 7×10^{14} ion cm^{-2}, the multilayered $Ni_{65}Mo_{35}$ alloy films were homogeneously mixed and uniformly vitrified.

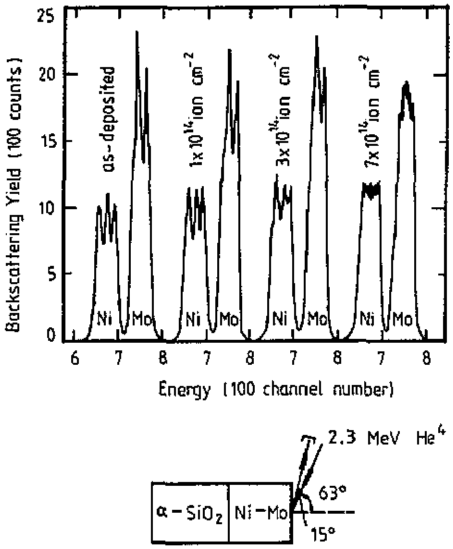

Figure 1. Backscattering spectra: as-deposited Ni–Mo films and samples irradiated to doses of 1, 3 and 7×10^{14} ion cm^{-2}, respectively.

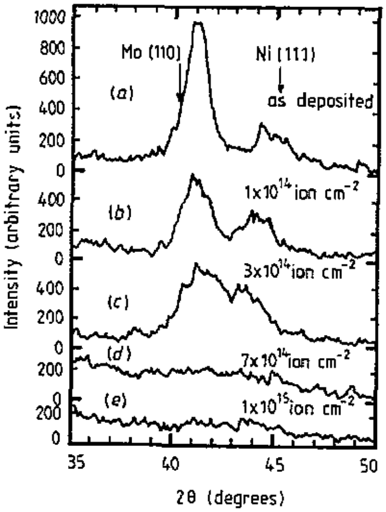

Figure 2. X-ray diffraction results: (*a*) as-deposited; (*b*) 1×10^{14} ion cm^{-2}; (*c*) 3×10^{14} ion cm^{-2}; (*d*) 7×10^{14} ion cm^{-2}; and (*e*) 1×10^{15} ion cm^{-2}.

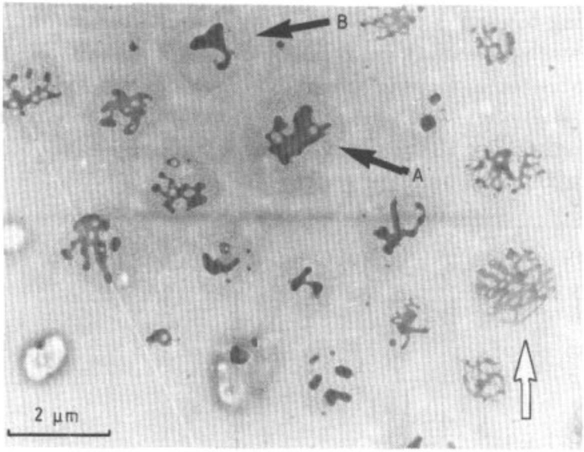

Figure 3. Disclinations formed in the $Ni_{65}Mo_{35}$ amorphous alloy films irradiated by xenon ions to a dosage of 7×10^{15} ion cm^{-2}. The dark appearance is the single crystalline metastable phase mediated by the interaction of the line defects.

3.2. Loops of odd lines and identification

A key idea of this study, which has not been carefully studied before, is to see what will happen to the as-vitrified structures if subjected to some additional doses of ion irradiation. As was expected, when the dose reached 7×10^{15} ion cm^{-2}, a remarkably odd morphology was observed, i.e. a large number of random loops of dark lines appeared in the amorphous matrix. Whereas two neighbouring doses, i.e. a lower dose of 5×10^{15} ion cm^{-2} and a higher one of 1×10^{16} ion cm^{-2}, both led to homogeneous amorphous phases. It is clearly seen in figure 3, a bright field image, that the randomly shaped loops seemed to be distributed homogeneously in the films. Each separate pattern consists of two sets of enclosed curves being differentiable everywhere. Many small hole-like patterns were surrounded by a large enclosed curve with an extremely random shape. The width of the dark lines was easily measured and ranged from 2 to 15 nm. The precipitates with a dark appearance in the space between these two enclosed curves, as noted by open arrows in figure 3, were identified to be the metastable phase described earlier by us [5]. All these patterns are located in a greyer basin than the surrounding matrix. The compositions of the dark precipitates, the grey basin, and the surrounding matrix were approximately $Ni_{50}Mo_{50}$, $Ni_{55}Mo_{45}$, and $NI_{65}Mi_{35}$, respectively, as determined by EDS measurement.

As shown in figure 3, the dark line contrast in different basins varied largely from one case to another. The loops with relative high and low contrasts are identified by full arrows A and B, respectively. Clearly, the dark lines marked B were hardly distinguishable. But the line contrast for a similar set of loops in a basin seemed to be uniform. By examining many different basins, it was found that each took on a different shape, and no specific symmetry could be attributed to the fat basins with random outlines. Figure 4 demonstrates a single set of loops at a higher magnification than that used in figure 3. The typical fringe morphology of amorphous structures can be readily identified in this bright field image, and no topological difference can be distinguished on either side of the dark lines. Electron diffraction analysis was conducted at three different areas marked A, B and C in figure 4. The corresponding diffraction patterns (DP) are shown in figures 5(*a*)–(*c*). Circle A in figure 4 concentrated on the dark precipitate and its DP in figure 5(*a*) was composed of sharp diffraction spots and a few diffuse halos from the amorphous matrix. This indicated that the dark precipitate was in a single crystalline state, and its dark contrast resulted from the diffraction deviation of the incident electron beam as it went through the crystalline precipitate. Circle C in figure 4 only enclosed the fringe regime away from the loops, and the corresponding DP in figure 5(*c*) consisted of several halos, indicating again the amorphous state of the uniform matrix. Finally, the diffraction pattern from the area including the segments of dark lines, as shown by circle B in figure 4, was also widely diffused halos (figure 5(*a*)) without any difference from that of the amorphous matrix. This fact demonstrated that no detectable small crystals decorated the dark lines. In other words the region including the dark lines was still in the amorphous state. For comparison, sharp diffraction rings from the invitrified films are shown in figure 5(*d*), indicating the coexistence of the polycrystalline Ni and Mo metals. It can be easily seen that the first amorphous halos shown in figures 5(*a*)–(*c*) are just located around the first two diffraction rings, Ni (111) and Mo (110), of the crystalline phases. From these diffraction results it can also be deduced that the contrast of the grey basins originated from differences in the atomic concentration and not from some kind of diffraction deviation.

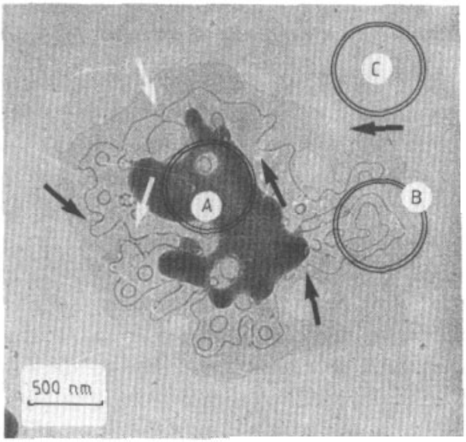

Figure 4. Bright field image of a set of magnified disclination loops. Full arrows indicating the fine voids. Open arrows specifying the tendency of self-reaction. Circles indicating the diffraction regions.

Scrutinizing figure 4 revealed another critical fact—that there were some fine white spots (about 25 nm in diameter) scattered in the amorphous matrix, and many of these were only located on the dark lines. As has been seen, the amorphous alloy films in this study were formed by the ion mixing technique. The dynamic collision process during energetic ion irradiation may generate a large number of defects [7] such as vacancies and aggregation of multi-vacancies will induce the formation of voids. In the area of the voids, the thicknesses of the films were thinned by the vacancy, and their (mass–depth) contrast in the bright field image would be white as in the case of crystalline solids. If a void was sufficiently small (say 30 nm in diameter), its fringe usually had a dark contrast due to the special diffraction geometry [7]. These inferences were in good agreement with our observations, and thus the fine spots appearing in the amorphous matrix were attributed to the small voids induced by ion irradiation. When the films

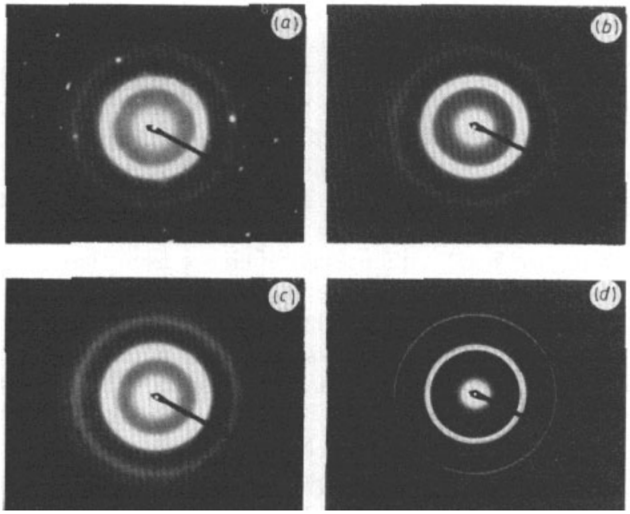

Figure 5. Electron diffraction patterns: (a)–(c) corresponding to the circled areas as shown in figure 4, indicating single crystals of the dark precipitate, and the amorphous structure of the matrix and the area including the disclination lines. (d) Polycrystalline rings before vitrification of the Ni–Mo films for comparison.

were irradiated to a higher dosage, e.g. 1.5×10^{16} ion cm^{-2}, the white voids became more evident. The density of the voids was also greatly increased, as shown in figure 6. The inset in figure 6 illustrates the diffraction pattern from the corresponding matrix. A few wide halos also indicated an amorphous state. In addition, a small diffuse ring was found within the first Ni–Mo amorphous halos in contrast with figures 5(a)–(c). The small ring was thought to result from the precipitation of over-saturated xenon atoms in the matrix. From this evidence, the dark loops cannot be the outline of voids in the ion mixed amorphous matrix. Moreover, a flat and extremely low contrast surface, as revealed by *in situ* SEM, showed that the dark lines were not from some kind of steps on the film surface either. From this, it can be deduced that the anomalous dark contrast loops were an intrinsic manifestation of the amorphous matrix.

Further TEM examination showed that as the sample was tilted with respect to the incident electron beam the relative contrast of loops in different basins changed in two different ways, i.e. some of them increased and others decreased, even disappeared. It was also observed that the line contrast became slightly more pronounced with a smaller objective aperture, and that a slight defocus seemed to widen and diffuse the dark lines. It is worthwhile pointing out that once a set of loops was visible its topological shape was invariant with the external conditions, and its contrast was almost uniform for the same set of loops. Dark field TEM examination revealed that the line loops in the bright field image turned into white line loops with the same geometry. We can therefore conclude that the interesting images resulted from the linear defects, i.e. disclination loops in the amorphous structures as predicted by Rivier *et al* [3].

To date, however, little is known about these defects, except that they are supposed to be established in the process of bond forming and breaking as atoms move [2]. As for the specific scheme of producing amorphous phases in our case, the dynamic collision

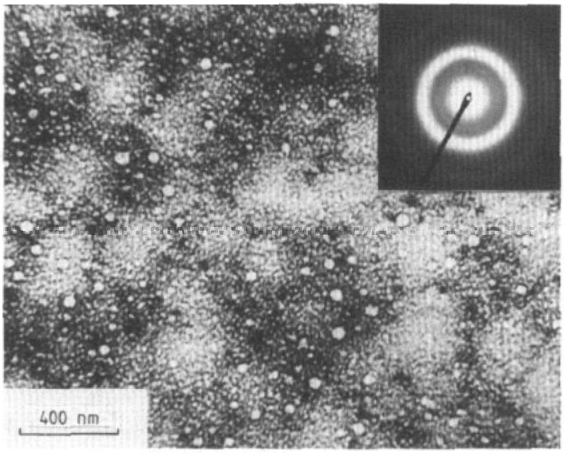

Figure 6. Voids in a TEM bright field image observed in the samples irradiated to 1.5×10^{16} ion cm^{-2}, the inset indicating the corresponding electron diffraction pattern.

process during energetic ion irradiation can stimulate the amorphous structures to a highly energetic intrinsic state, at which atoms and defects (mainly point defects) have a larger mobility, and hence are sufficiently able to perform such bond forming and breaking processes so as to rearrange themselves in a large scale. As is well known, disclination is a one-dimensional topological defect with a typical atomic distance. The visual width (2–15 nm) observed in the TEM bright field image was mainly caused by the surrounding stress field, and was of the same order as that of dislocations in crystals (3–10 nm). As a consequence, the line defect could be recorded by a TEM with a not extremely high resolution [10, 11]. Furthermore, because of the opposite effect of stress distortion of the amorphous networks, the visual position of the disclination would have a displacement (about the same order of its width) from its virtual location in the matrix. In most cases, therefore, a narrow white contrast band appears preferentially on one side of dark disclination lines, as can be seen by careful examination of figure 4. This notwithstanding, how the disclination lines were first initiated in the random networks of amorphous structures through the dynamic process and how the atoms arranged themselves locally around the linear defect certainly deserves further well-designed experimental investigation.

3.3. Contrast formation of disclination lines

First, considering a plane electron wave ($\boldsymbol{K}_{\mathrm{i}}$) is incident normally on a film surface, the scattering amplitude in the observation direction $\boldsymbol{K}_{\mathrm{f}}$ is given (in electron units) by [9] the summation of the amplitude from each atom i, having a position $\boldsymbol{r}$,

$$\Phi_{\mathrm{s}}(\boldsymbol{K}) = \sum_i f_i \cdot \mathrm{e}^{2\pi \mathrm{i} \boldsymbol{K} \cdot \boldsymbol{r}} \tag{1}$$

where $\boldsymbol{K} = \boldsymbol{K}_{\mathrm{f}} - \boldsymbol{K}_{\mathrm{i}}$. For the elastic scattering, $|\boldsymbol{K}_{\mathrm{f}}| = |\boldsymbol{K}_{\mathrm{i}}|, |\boldsymbol{K}| = 2\pi \sin\theta/\lambda, 2\theta$ is the scattering angle. The scattered intensity is simply $\Phi_{\mathrm{s}}(\boldsymbol{K})^{*}\Phi_{\mathrm{s}}'(\boldsymbol{K})$. Expression (1) is known to be true for all materials whether crystalline or amorphous [9].

In the Column approximation [10], the scattered amplitude due to the atoms in the depth element $z \rightarrow z + \mathrm{d}z$ per unit film area in the direction $\boldsymbol{K}_{\mathrm{f}}$ can be expressed by

$$\mathrm{d}\phi_{\mathrm{s}}(\boldsymbol{K}) = A\mathrm{e}^{2\pi\mathrm{i}\boldsymbol{K}\cdot\boldsymbol{r}}\,\mathrm{d}z \tag{2}$$

where the coefficient A may be relevant to the atomic scattering factor f_i and the number density of atoms ρ, which is reasonably supposed to be independent of the depth z. The existence of a defect will cause some distortion of its neighbouring area. The amplitude of the scattering electron wave by the depth element $\mathrm{d}z$ in a deformed area is described by

$$\mathrm{d}\phi_{\mathrm{s}}^{\mathrm{d}}(\boldsymbol{K}) = A\mathrm{e}^{2\pi\mathrm{i}\boldsymbol{K}\cdot\boldsymbol{r}'}\,\mathrm{d}z \tag{3}$$

where $\boldsymbol{r}' = \boldsymbol{r} + \Delta\boldsymbol{r}$. The scattered vector $\boldsymbol{K}$ represents the diffraction geometry, and is assumed to be invariant under a defined direction of observation $\boldsymbol{K}_{\mathrm{f}}$. In our nearly two-dimensional case, a disclination loop is assumed to be located entirely at a depth of y. The total scattered amplitude due to a disclination line can be written as

$$\phi_{\mathrm{s}}^{\mathrm{d}} = AC\int_0^t \mathrm{e}^{\mathrm{i}(\alpha-\beta z/x)}\,\mathrm{d}z \tag{4}$$

where the distance parameter $\beta = -2\pi\boldsymbol{K}_z x$, $C = \exp[-2\pi\mathrm{i}(\boldsymbol{K}_x x + \boldsymbol{K}_y y)]$, and $|c|^2 = 1$. t is the film thickness. Clearly, it is the additional phase factor

$$\alpha = 2\pi\boldsymbol{K}\cdot\Delta\boldsymbol{r} \tag{5}$$

that leads to the contrast of the line defects. Accordingly, the contrast formalism of the disclination loops in amorphous films is analogous to that of dislocations in crystalline materials [11]. This is why the line contrast of the disclination was considerably affected by the incident geometry ($\boldsymbol{K}$). The contrast variation among sets of loops might be caused by different displacement ($\Delta\boldsymbol{r}$) of the line defect. Furthermore, if $\boldsymbol{K}\cdot\Delta\boldsymbol{r} = 0$, then $\alpha = 0$, the disclination becomes invisible, which is also qualitatively in accordance with our observations.

4. Self-consistent elucidation of disclination loops

In the previous sections, we have addressed the evidence for the appearance of disclination loops in Ni–Mo amorphous films, and accounted for their contrast features both experimentally and theoretically. However, many other distinguished features pertinent to the observed disclination remain unclear. For instance, why did the defect loops in the amorphous films manifest themselves as two sets of enclosed curves being differentiable almost everywhere, and why did a metastable crystal prefer to precipitate along the spacing between the two enclosed curves? In addition, what was responsible for the self-avoidance of the defect lines? And essentially, what made the defect line crumble randomly instead of being a single homogeneous circle-like loop. The following part is devoted to elucidating these intriguing questions.

4.1. Statics and dynamics of defect evolution

Provided that the uniformly mixed amorphous film is an elastic continuum media, *the differentiation of a defect line will be a direct consequence of spatial continuity.* Explicit argument of gauge theory indicates that only 2π-disclinations exist in amorphous structures [3, 8, 12]. This means that a local frame always rotates 2ϕ on going around a disclination, as illustrated in figure 7(*a*), where $\boldsymbol{T}(\boldsymbol{r})$ is a unit tangent vector at the position $\boldsymbol{r}$ on a defect line. Consequently, a disclination loop can be represented by a set of tangent vectors $\{\boldsymbol{T}(\boldsymbol{r})\}$. Furthermore, the interaction between two neighbouring defect elements in a plane can be approximately written as [2, 13]

$$f \propto \frac{\boldsymbol{T}(\boldsymbol{r}_1)\cdot\boldsymbol{T}(\boldsymbol{r}_2)}{|\boldsymbol{r}_1-\boldsymbol{r}_2|}. \tag{6}$$

This means that like pairs, i.e. $\boldsymbol{T}(\boldsymbol{r}_1) \parallel \boldsymbol{T}(\boldsymbol{r}_2)$, repel, and unlike pairs, $\boldsymbol{T}(\boldsymbol{r}_1) \parallel -\boldsymbol{T}(\boldsymbol{r}_2)$, attract. Equation (6) is the basis for the following discussion.

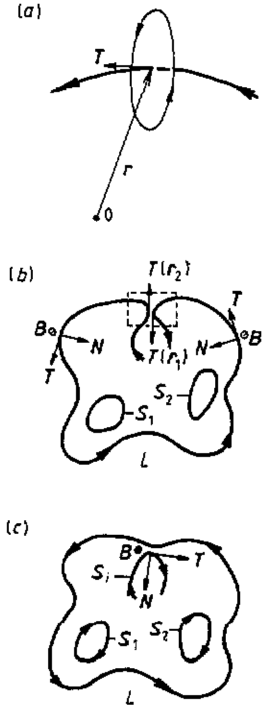

Figure 7. Illustrative defect lines: (*a*) tangent vector and local environment of a disclination line; (*b*) and (*c*) configuration of the defect loops before and after an attractive reaction takes place.

Furthermore, the observed differentiation or smoothness implies that the derivative, $\boldsymbol{T}'(\boldsymbol{r}) = |\boldsymbol{T}'(\boldsymbol{r})|\boldsymbol{N}(\boldsymbol{r})$, exists. $\boldsymbol{N}(\boldsymbol{r})$ is the unit normal at $\boldsymbol{r}$ satisfying $\boldsymbol{T}(\boldsymbol{r})\cdot\boldsymbol{N}(\boldsymbol{r}) = 0$. According to the classical theory of differential geometry [14], the corresponding unit subnormal is defined by $\boldsymbol{B}(\boldsymbol{r}) = \boldsymbol{T}(\boldsymbol{r}) \times \boldsymbol{N}(\boldsymbol{r})$. In our case of an approximately two-dimensional film, all defect loops were confined to being parallel to the film surface. The vector $\boldsymbol{B}(\boldsymbol{r})$ can only be directed out of or into the film plane, and the corresponding defect loops were denoted by L and S, respectively. We assume that each randomly shaped large loop is an L type, as shown in figure 7(*b*). Looking at the broken square in figure 7(*b*), the attractive force ($f < 0$) between $\boldsymbol{T}(\boldsymbol{r}_1)$ and $\boldsymbol{T}(\boldsymbol{r}_2)$ increases drastically as $\boldsymbol{r}_1$ approaches to $\boldsymbol{r}_2$. If $|\boldsymbol{r}_1 - \boldsymbol{r}_2| \to 0, f \to \infty$, then a reaction

$$\lim_{\boldsymbol{r}_1 \to \boldsymbol{r}_2} (\boldsymbol{T}(\boldsymbol{r}_1) + \boldsymbol{T}(\boldsymbol{r}_2)) = 0 \tag{7}$$

takes place, which results in the formation of an inner enclosed S-type curve and the self-avoidance of the defect loops, as illustrated in figure 7(*c*). The analogous procedure as shown in figure 7 can indeed be observed in the practical patterns, as specified in figure 4 by open arrows. Therefore, a developed linear defect always consists of two sets of loops, one L-type and many S-types ($S = \cup_i S_i$) ones in it (L). This inference is exactly in accordance with our observations.

In fact, considering the defect line in amorphous structures as a one-dimensional elastic manifold embedded in three- or two-dimensional space, the self-avoiding behaviour is therefore a straightforward result of a continuum theory of crumpled manifolds [15]. In our case, however, the self-avoidance was induced by the very attractive self-reaction (equation (7)) on contact, instead of a simple repulsion as studied earlier [15].

As previously stated, there were small amounts of fine voids dispersed in the amorphous matrix. The surrounding networks of these voids would be deformed relative to the previous cases and would thus introduce a local stress field. When the disclination lines approached the white voids, their two stress fields would interact with each other. The voids usually acted as unmovable objects and pinned the defect lines. Therefore, it was believed that the randomly located fine voids, their pinning effect and the linear tension along the defect lines were responsible for the irregular crumbling, and then the very self-reaction of disclination loops.

4.2. Defect mediated precipitation

The movement and the reaction of defect lines would eventually split a total amorphous film into two distinctly energetic regions. The regions between the two types of loop have been relaxed to a low energy state by the sweep of the defect lines. The total free energy E in these regions, where an attractive force dominates, is assumed to be $E < 0$. In contrast, the unscanned or unrelaxed areas both outside the L-type loops and inside the S-type loops are at a high energy state with a total energy $E > 0$, which corresponds to the repulsion field. While the free energy of the metastable and equilibrium crystalline phases in this system are represented by E_{m} and E_{c} ($E_{\mathrm{c}} < E_{\mathrm{m}} < 0$), respectively. In the attractive regions ($E < 0$), only if the free energy E, say $E_i, < E_{\mathrm{m}}$, can the metastable phase nucleate under the driving force $\Delta G = E_{\mathrm{m}} - E_i$. While $E > E_{\mathrm{m}}$, the metastable phase cannot nucleate even within the attractive areas with $E < 0$. Apparently, the equilibrium crystalline phase (E_{c}) is hard to nucleate in the relatively weak interaction field of linear defects. The excess energy (in heat form) during amorphous-to-crystalline phase transformation, i.e. the growth of metastable phases, will certainly enhance the precipitation process again. This is probably the reason why only the metastable phase precipitates in most cases in the spacing between the two enclosed curves, and sometimes goes beyond the spacing as shown in figure 3.

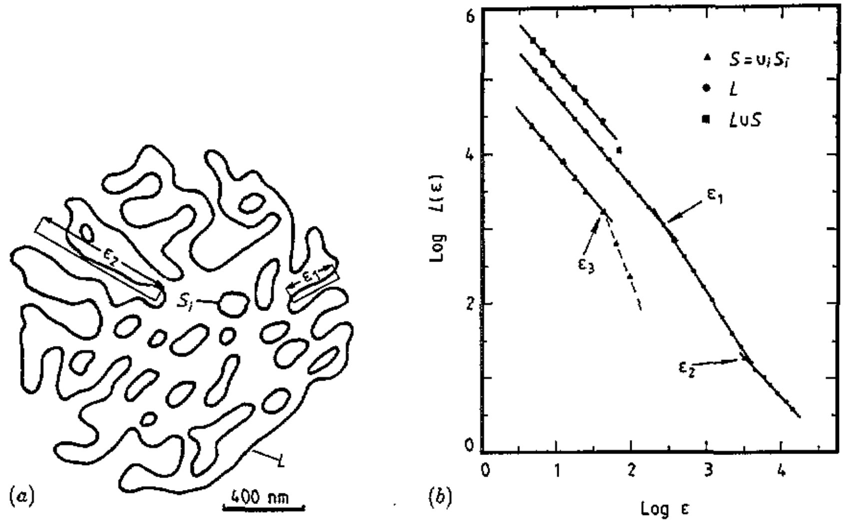

Figure 8. (*a*) An example of digitized disclination loops for fractal analysis. (*b*) Log–log plot of the maximum relative length $L(\epsilon)$ against the scale ϵ for the disclination shown in (*a*). The full circles indicating the results for the L-type loop, the triangles for the set of loop $S_i(S = \cup_i S_i$, and the squares for the whole disclination loop $(L \cup S)$.

5. Fractal nature of disclinations

It is well known that a fractal geometry has recently been developed as a powerful means of characterizing a variety of random systems [16]. The fractal structure of randomly shaped disclination loops is studied in terms of computer image processing. A set of disclination loops, one of which is shown in figure 8(*a*), was firstly extracted from a magnified electron micrograph, and then was digitized with a VAX image processor at 512 pixel × 512 pixel resolution. Any practical fractal structure will have a lower and an upper length scale cutoff. In the present case the width of disclination line, $\delta = 10$ nm, which corresponds to 2 pixel, is the lower cutoff ϵ_{min}. The upper cutoff is given by the linear dimension $\epsilon_{\max}$ of the L-type loop. Figure 8(*b*) shows the log–log plot of the relative length $L(\epsilon)$ in the scale of ϵ; the full circles indicate the results for the L-type loops in figure 8(*a*). Apparently, there are two crossovers at ϵ_1 and ϵ_2 in figure 8(*b*), which divide the whole experimental data into three regions. Each of them can be well fitted by a straight line. As for a fractal curve, the relative length satisfies

$$L(\epsilon) \propto \epsilon^{-D} \qquad (8)$$

where D is called its fractal dimension. The relative perimeter $L(\epsilon)$ here is a maximum value obtained from more than ten reference points randomly taken on the disclination loop. The fractal dimension, as measured in the regions of $\epsilon_{\min} < \epsilon < \epsilon_1, \epsilon_1 < \epsilon < \epsilon_2$, and $\epsilon_2 < \epsilon < \epsilon_{\max}$ are 1.20, 1.44 and 1.16, respectively. The uncertainty in fractal dimensions, as estimated from the fit in figure 8(*b*), is about ±0.02. However, taking into account the error occurring in image processing and some other procedures, a more realistic error bar is at most ±0.06. Computer analysis showed that the lower crossover ϵ_1 measures the average depth of the disclination fjords, while the higher one ϵ_2 corresponds to their maximum depth, as indicated in figure 8(*a*).

In the region of the scale $\epsilon > \epsilon_2$, all fjords are smeared out, the fractal dimension of $D_3 = 1.16$ mostly revealed the outline of the L-type loop. It is in this sense that the disclination of the L-type loop seems to be a self-affine fractal [17], for which one must distinguish between local and global fractal dimensions. Whereas in our case, there are two local fractal dimensions D_1 and D_2. The fitting result of the S-type loop is also denoted in figure 8(*b*) by full triangles. The most striking thing is that in the scale range of $\epsilon_{\min} < \epsilon < \epsilon_3$, the union set $S = \cup_i S_i$ of separate loops (S_i) is also self-similar with a fractal dimension D being exactly the same as that of the L-type loop in the low region of scale ϵ. Therefore, the total disclination, i.e. $L \cup S$, was also scale invariant with the same fractal dimension $D = 1.20$, as indicated in figure 8(*b*) by full squares. The same fact was found to be true for all digitized disclination loops (more than ten), which demonstrated the existence of a universal fractal dimension $D_f = 1.20 \pm 0.06$. This value, we believe, characterizes the underlying nature of the self-avoiding disclination loops, while the fractal dimension D_2 in the region of $\epsilon_1 < \epsilon < \epsilon_2$, varied from 1.20 to 1.80 for different cases. In the low limit of D_2, an L-type loop behaves like a statistically self-similar fractal curve in nearly the whole range of length scale.

The scaling structure of a random surface has been a subtle and fascinating subject for fractal study. Stanley *et al* [18] argued that the fractal dimension D_f of the total perimeter is higher than that of the external perimeter. In our case, however, they are all equal to each other in the low scale range. This, in fact, is quite reasonable in the sense that either the L-type loop or the S-type loop is an independent physical object, i.e. a line defect, in amorphous structures, instead of an external or internal surface of some other object if it existed. From the first part of this paper, we know that each Si loop had always been a segment of an L-type loop before the *i*th reaction occurred. The dominant differences between the two types of loops is the global direction of their subnormals, and there is no reason why this should affect their subtle scaling structures. If we visualize the relaxed area between the L- and S-type loops as an independent physical object such as a new phase, no meaningful scaling results could be found from the digitized pattern.

6. Conclusions

By irradiating the as-vitrified $Ni_{65}Mo_{35}$ films to a critical dose, many one-dimensional topological defects, i.e. disinclination loops, were formed in the amorphous matrix. The defect lines featured two types (L and S) of loop. It was found that point-like defects, i.e. randomly localized fine voids in our case, and the attractive self-reaction governed the evolution behaviour of the defect lines, and therefore induced the irregular geometrical shape. Metastable crystalline precipitation is direct evidence for the defect-mediated phase transition [19]. The scaling analysis of disclination loops reveals a universal fractal dimension $D_f = 1.20 \pm 0.06$, which well characterizes the subtle structures of the line defects in amorphous matter. A better understanding of the disclination loops remains a challenge for further theoretical consideration and computer simulation.

Acknowledgments

We are grateful to Dr J G Sun, Dr J Zhu, and Professor K H Kuo for helpful discussions. The staffs of the TEM Laboratories of Beijing University and the Analysis

Centre of Tsinghua University are also acknowledged for their assistance. This work was supported by the National Natural Science Foundation of China and the International Atomic Energy Agency (Research Contract No 4731/R3/RB).

References

[1] Priedel J 1979 *Disclination in Solids* vol 1, ed F R N Nabarro (Amsterdam: North-Holland) p 1
[2] Venkatarama G and Sahoo D 1985 *Contemp. Phys.* **26** 35; 1986 *Contemp. Phys.* **27** 1
[3] Rivier N 1979 *Philos. Mag.* A **40** 859
Rivier N and Duffy D M 1982 *J. Physique* **43** 293
[4] Sadoc J F and Rivier N 1987 *Philos. Mag.* B **55** 537
Bohsung J and Trebin H R 1987 *Phys. Rev. Lett.* **58** 1204
[5] Liu B X 1986 *Phys. Status Solidi* a **94** 11
Liu B X, Johnson W L, Nicolet M A and Lau S S 1983 *Nucl. Instrum. Methods* **209/210** 229
[6] Shang C H and Liu B X 1989 *Nucl. Instrum. Methods in Phys. Res.* B **37/38** 420
[7] Thompson M W 1969 *Defects and Radiation Damage in Metals* chs 4 and 5 (Cambridge: Cambridge University Press)
[8] Rivier N 1983 *Topological Disorder in Condensed Matter* ed F Yonezawa and T Ninomiya (Berlin: Springer) p 14
[9] Elliott S R 1983 *Physics of Amorphous Materials* (Harlow: Longman) p 53
Cowley J M 1975 *Diffraction Physics* (Amsterdam: North-Holland)
[10] Whelan M J 1970 *Modern Diffraction and Imaging Techniques in Material Science* ed S Amelinckx, R Gevers, G Remaut and J Van Landuyt (Amsterdam: North-Holland) p 62
[11] Hirsch P B, Howie A, Nicholson R B, Pashley D W and Whelan M J 1967 *Electron Microscopy of Thin Crystals* chs 13, 15, 18 (London: Butterworth)
[12] Duffy D M 1981 *PhD Thesis* Imperial College, University of London
[13] Chandrasekhar S and Ranganath G S 1986 *Adv. Phys.* **35** 5
[14] Hicks N J 1965 *Notes on Differential Geometry* (Princeton: D Van Nortrand)
[15] Kardar M and Nelson D R 1987 *Phys. Rev. Lett.* **58** 1289
Duplantier B 1987 *Phys. Rev. Lett.* **58** 2733
[16] Mandelbrot B B 1982 *The Fractal Geometry of Nature* (New York: Freeman)
[17] Feder J 1984 *Fractals* A **17** L373
Mandelbrot B B 1985 *Phys. Scr.* **32** 257
[18] Stanley H E 1986 *Fractals in Physics* ed L Pietronero and E Tosatti (Amsterdam: Elsevier) p 327
Bunde A, Herriman H J, Margolina A and Stanley H E 1985 *Phys. Rev. Lett.* **5** 653
[19] Nelson D R 1983 *Phase Transitions and Critical Phenomena* ed C Domb and J L Lebowitz (New York: Academic) pp 2–93